

# Geophysical Research Letters®

## RESEARCH LETTER

10.1029/2022GL097812

### Key Points:

- Medium energy electrons can directly impact the mesospheric temperature and winds
- During a sudden stratospheric warming event, even weak geomagnetic activity can alter the mesospheric wind fields
- Mesospheric  $O_3$  decrease modulates gravity wave filtering and leads to a dynamical response during unstable atmospheric conditions

### Correspondence to:





H. N. Tyssøy,  
hilde.nesse@uib.no

### Citation:

Zúñiga López, H. D., Tyssøy, H. N., Smith-Johnsen, C., & Maliniemi, V. (2022). The direct effect of medium energy electron precipitation on mesospheric dynamics during a sudden stratospheric warming event in 2010. *Geophysical Research Letters*, 49, e2022GL097812. <https://doi.org/10.1029/2022GL097812>

Received 18 JAN 2022  
Accepted 26 MAY 2022

## The Direct Effect of Medium Energy Electron Precipitation on Mesospheric Dynamics During a Sudden Stratospheric Warming Event in 2010

Héctor Daniel Zúñiga López<sup>1</sup> , Hilde Nesse Tyssøy<sup>1</sup> , Christine Smith-Johnsen<sup>1</sup> , and Ville Maliniemi<sup>1</sup> 

<sup>1</sup>Birkeland Centre for Space Science, Department of Physics and Technology, University of Bergen, Bergen, Norway

**Abstract** Medium energy electron (MEE) (30–1,000 keV) precipitation enhances the production of nitric ( $NO_x$ ) and hydrogen oxides ( $HO_x$ ) throughout the mesosphere, which can destroy ozone ( $O_3$ ) in catalytic reactions. The dynamical effect of the direct mesospheric  $O_3$  reduction has long been an outstanding question, partly due to the concurrent feedback from the stratospheric  $O_3$  reduction. To overcome this challenge, the Whole Atmosphere Community Climate Model version 6 is applied in the specified dynamics mode for the year 2010, with and without MEE ionization rates. The results demonstrate that MEE ionization rates can modulate temperature, zonal wind and the residual circulation affecting  $NO_x$  transport. The required fluxes of MEE to impose dynamical changes depend on the dynamical preconditions. During the Northern Hemispheric winter, even weak ionization rates can modulate the mesospheric signal of a sudden stratospheric warming event. The result provides a first step in a paradigm shift for the understanding of the MEE direct effect.

**Plain Language Summary** Medium energy electrons (MEE) precipitate into the mesosphere, where they produce nitric ( $NO_x$ ) and hydrogen oxides ( $HO_x$ ), which are both associated with ozone ( $O_3$ ) loss. During polar winter,  $NO_x$  is long-lived and can be transported all the way down to the stratosphere, where it can lead to a stratospheric  $O_3$  loss, which has the potential to change the dynamics of the atmosphere. The dynamical impact of the mesospheric  $O_3$  loss is, however, unclear. To study the impact of MEE on the mesospheric dynamics, two Whole Atmosphere Community Climate Model runs are compared, with and without MEE ionization. This study shows that MEE have the potential to modulate the dynamics of the mesosphere directly. Furthermore, it shows that when the atmosphere is unstable, even weak ionization rates are able to modulate the signal of a sudden stratospheric warming in the mesosphere.

## 1. Introduction

The magnetosphere is constantly being ripped and torn by the solar wind, and part of this energy is guided by the Earth's magnetic field and deposited into the atmosphere as energetic electron precipitation (EEP) (Mironova et al., 2015). Auroral electrons (1–30 keV) from the plasma sheet ionize the lower thermosphere, whereas Medium Energy Electrons (MEE) (30–1,000 keV) from the radiation belts cause ionization throughout the mesosphere (Sinnhuber et al., 2012). The increased ionization initiates chemical reactions, increasing the production of nitrogen ( $NO_x$ ) and hydrogen oxides ( $HO_x$ ). Short-lived  $HO_x$  gasses will reduce mesospheric  $O_3$  in catalytic reactions (Andersson et al., 2014), here referred to as the MEE direct effect.

$O_3$  loss due to  $NO_x$  catalytic cycles is effective only below  $\sim 0.5$  hPa, mainly in the stratosphere (Lary, 1997). During polar winter, when no sunlight is present,  $NO_x$  can have an effective lifetime of months (Solomon et al., 1982). The winter polar vortex prevents  $NO_x$  from leaving high latitudes, and the residual circulation can transport  $NO_x$  all the way down to the stratosphere, which is called the EEP indirect effect (Maliniemi et al., 2020; Randall et al., 2007). Stratospheric and/or mesospheric ozone loss can lead to a significant polar vortex enhancement on a seasonal scale (Baumgaertner et al., 2011; Maliniemi et al., 2019; Salminen et al., 2019; Seppälä et al., 2013).

Andersson et al. (2014) demonstrated based on observations that even moderate geomagnetic activity was responsible for significant mesospheric  $O_3$  reduction in wintertime polar regions. The MEE direct impact on  $HO_x$  and  $O_3$  has been investigated in several subsequent observational studies (Zawedde et al., 2016, 2018, 2019). One of the first efforts to simulate the dynamical impacts of MEE was implemented by Codrescu et al. (1997), applying

© 2022. The Authors.

This is an open access article under the terms of the [Creative Commons Attribution-NonCommercial-NoDerivs License](https://creativecommons.org/licenses/by-nc-nd/4.0/), which permits use and distribution in any medium, provided the original work is properly cited, the use is non-commercial and no modifications or adaptations are made.

the Thermosphere Ionosphere Mesosphere General Circulation Model which showed  $O_3$  loss up to 27% followed by small changes in the temperature and wind field. Semeniuk et al. (2011) revealed up to 60%  $O_3$  depletion due to MEE in the Northern Hemisphere (80% in the Southern Hemisphere) winter, applying the Canadian Middle Atmosphere Model. The NH polar vortex strength showed a statistically significant increase below 30 km altitude, but no significant changes in the residual circulation were evident. Arsenovic et al. (2016) found local  $O_3$  decreased up to 35% associated with MEE, using the chemistry-climate model SOCOL3. These changes were followed by an intensification of the polar vortex, as well as mesospheric warming and stratospheric cooling. Furthermore, surface air temperature responses were detected in several regions.

Meraner and Schmidt (2018), however, rejected the possibility of a significant dynamical impact of the direct MEE effect based on the HAMMONIA model. They studied both the direct and indirect effect by artificially introducing a steady  $O_3$  reduction in the mesosphere and stratosphere separately. Guttu et al. (2020) applied the Whole Atmosphere Community Climate Model (WACCM) version 6 with and without MEE ionization rates, but largely limited their assessment to the stratospheric  $O_3$  changes, the indirect EEP effect, despite a relatively strong direct MEE  $O_3$  reduction in the mesosphere. The temperature and zonal wind anomalies found in the mesosphere were assumed to be a consequence of the stratospheric  $O_3$  reduction.

The above mentioned simulations apply models in free-running mode, which allows for dynamical feedback from the stratospheric EEP indirect effect. Furthermore, they show the chemical and dynamical response on a monthly or seasonal time scale. Hence, the initial temperature response in the mesosphere might be concealed by the subsequent dynamical feedback. Meraner and Schmidt (2018) showed a statistically significant temperature change in the opposite hemisphere for both the mesospheric and stratospheric  $O_3$  reduction cases. This was interpreted as an indication of inter-hemispheric coupling, which implies that the pole-to-pole circulation is impacted. If the pole-to-pole circulation is slowed down, it will result in a reduction of the adiabatic heating in the mesosphere and upper stratosphere, including the same altitudes where the initial  $O_3$  reduction is introduced. This renders the total temperature signal on monthly scales ambiguous and insignificant, as the initial temperature response is veiled by the subsequent dynamical change.

Asikainen et al. (2020) demonstrates, based on ERA-40/ERA-Interim reanalysis data, that EEP-related enhancement of the stratospheric polar vortex and other associated dynamical changes are seen only during winters when an SSW occurs and that the EEP-related changes are observed systematically, slightly before the SSW onset. They hypothesized that the increased planetary wave activity before the SSW favors enhanced wave-mean-flow interaction, which can dynamically amplify the initial polar vortex enhancement caused by the  $O_3$  loss. Furthermore, Salminen et al. (2020) show that EEP can significantly influence the occurrence rate of SSWs. The initial pre-conditions such as SSWs are, however, somewhat challenging to account for in the free-running mode, as the EEP impact itself and its dynamical feedback is expected to modulate them. A climate simulation run in a specified dynamics (SD) mode, where the stratosphere wind and temperature field in the troposphere and stratosphere are nudged, enables a unique insight into the role of the MEE direct effect in the mesosphere. It will ensure the same planetary and gravity wave forcing of the lower mesosphere for different model run ensemble members, regardless of the dynamical feedback of the EEP indirect impact. Note, however, that the SD mode cannot be used to study the stratospheric response to MEE. The observed stratospheric dynamics might be affected by the actual MEE forcing, which could render the model projection to be dynamically inconsistent with the stratospheric observations.

The chemistry climate model WACCM version 6 now includes a more sophisticated chemical scheme, which improves the complicated ion chemistry related to  $NO_x$  and  $HO_x$  production and losses in the mesosphere (Andersson et al., 2016; Verronen et al., 2016). To investigate the MEE direct effect of the atmospheric chemistry and dynamics, two WACCM runs in the SD mode for the year 2010 have been studied, one including both auroral and MEE forcing (the MEE run) and one including only auroral forcing (the noMEE run). The year 2010 marked the end of the deep solar minimum of solar cycle 24. Furthermore, it includes an SSW in January, while the rest of the year is dynamically stable.

## 2. Methods

### 2.1. WACCM

WACCM is a global chemistry-climate model, developed by the National Center for Atmospheric Research (NCAR) (Hurrell et al., 2013). The model version used in this study is WACCM6 (Gettelman et al., 2019), which extends from the surface up to about  $6 \cdot 10^{-6}$  hPa ( $\sim 140$  km geometric height), with 88 pressure levels and a horizontal resolution of  $0.95^\circ$  latitude by  $1.25^\circ$  longitude. WACCM6 is able to reproduce the observed climatology of temperatures, winds and trace constituents in the middle atmosphere, as well as to reproduce stratospheric variability from SSWs (Gettelman et al., 2019; Marsh et al., 2013).

In the Specified Dynamics (SD) version of WACCM, wind and temperatures are nudged with reanalysis data from the NASA Global Modeling and Assimilation Office's Modern-Era Retrospective Analysis for Research and Applications (MERRA) 2 (Rienecker et al., 2011), by the method described in Kunz et al. (2011). The model is nudged from the surface up to  $\sim 50$  km ( $\sim 1$  hPa), with a transition region from  $\sim 50$  to  $\sim 60$  km, and free running above  $\sim 60$  km. WACCM-SD is effective for reducing biases in the winds and temperatures and climate noise, and reproducing the chemical response to specific events.

The WACCM-D variant includes an improved representation of the ion-chemistry in the D-region, which ultimately leads to more effective NO production in the mesosphere. It is based on a simplification of the Sodankylä Ion and Neutral Chemistry and includes 20 positive ions and 21 negative ions, which enables 307 reactions in the mesosphere (Verronen et al., 2016).

In WACCM6, the ionization from auroral electrons ( $< 30$  keV) is parametrized by the Kp-index. The energy spectrum has a Maxwellian distribution with a fixed characteristic energy of 2 keV. Due to the fixed characteristic energy, the resulting ionization rate profile always peaks at around 110 km. In general, the energy deposition from auroral electrons is limited to altitudes above 95 km (Roble et al., 1987). Furthermore, the upper boundary of WACCM6 is the three-dimensional Nitric Oxide Empirical Model in the lower thermosphere. The model is parametrized by the Kp-index and the 10.7 cm solar radio flux (F10.7), based on NO observations between 97.5 and 150 km made by the Student NO Experiment satellite (Marsh et al., 2004).

WACCM6 is the first version of the climate model that by default includes MEE. The MEE precipitation accounts for the ionization from radiation belt electrons, with energies ranging from 30 to 1,000 keV. The MEE ionization is parametrized by the geomagnetic Ap-index, and the ionization model is based on observations from the  $0^\circ$  detector from the Medium Energy Proton/Electron Detector instrument on board Polar Orbiting Environmental Satellites. The energy-flux spectrum of the precipitating electrons has a time resolution of one day. The ionization rates are typically found at altitudes between 70 and 110 km, with the peak ionization rate found at about 90 km (van de Kamp et al., 2016).

### 2.2. WACCM Model Runs

To study the effects of MEE in WACCM, two runs have been performed in the SD mode including the D-region ion chemistry (Verronen et al., 2016). The only difference between the two runs is the ionization rate input from the medium energy electron precipitation. The “noMEE” case includes only ionization rates from precipitating auroral electrons, while the “MEE” case includes ionization rates from both precipitating auroral electrons and medium energy electrons. All data shown in this study corresponds to the Northern Hemisphere during the year 2010. The data has been averaged over the latitude band from  $60$  to  $70^\circ$ N with a daily resolution.

## 3. Results

The year 2010 is characterized by a transition from the deep solar minimum to the ascending phase of solar cycle 24. This is also reflected in the geomagnetic Ap index which displays low levels of activity until April (the upper panel of Figure 1). The subsequent panels show the NO volume mixing ratio (VMR) and zonal wind for the MEE (blue line) and noMEE case (green line), along with their differences (black line). The differences in NO correspond well in time with geomagnetic activity (high Ap), and as expected, the MEE case has higher NO concentrations than the noMEE case. The largest difference in NO concentration is, however, found in January, where Ap shows little activity. During this period the noMEE case surprisingly also shows more NO than the MEE case

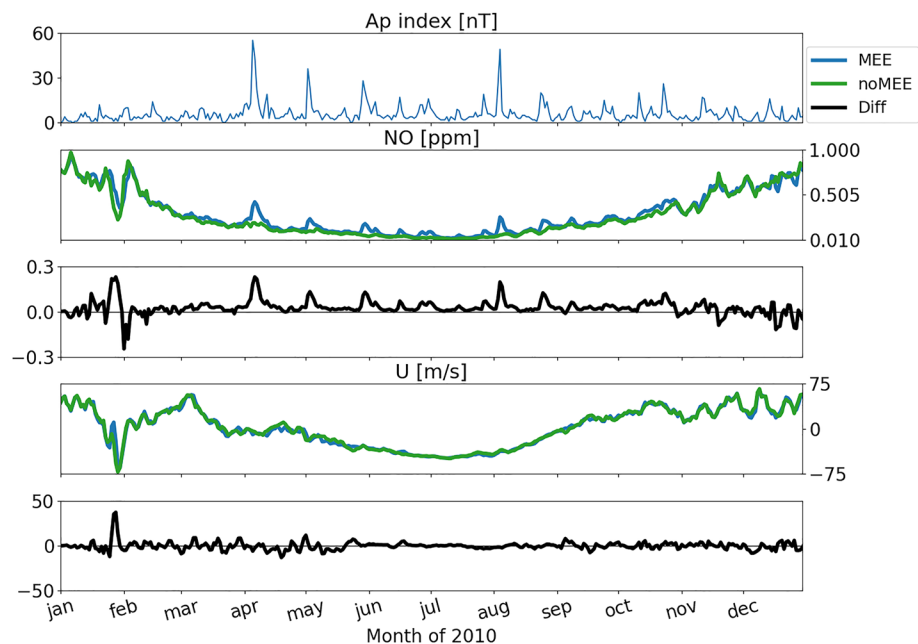


**Figure 1.** The first panel corresponds to the Ap index (geomagnetic activity). The second and third panel correspond to the NO concentration between  $10^{-3}$  hPa and  $10^{-2}$  hPa, averaged over the latitude band  $60\text{--}70^\circ\text{N}$  for both the Medium energy electrons (MEE) (blue line) and no-MEE (green line) run, as well as their difference (black line). The fourth and fifth panel correspond to the zonal wind velocity between  $10^{-1}$  hPa and  $10^{-2}$  hPa, averaged over the latitude band  $60\text{--}70^\circ\text{N}$  for both the MEE (blue line) and no-MEE (green line) run, as well as their difference (black line).

for several days. At the same time, the zonal wind reverses corresponding to an SSW (as seen in Figure 2 around 1 hPa). Here, the maximum zonal wind difference is found to be almost 40 m/s between the MEE and noMEE case. No comparable large differences in zonal wind are seen at other times of the year.

The wind reversal in the lower mesosphere is associated with the major SSW with the central date of 23 January 2010 (Jia et al., 2016). Figure 2 shows the zonal wind velocity for both the noMEE (upper panel) and the MEE (lower panel) case. 23 January is marked as day zero. Positive velocities correspond to eastward zonal winds, typical for the stratospheric polar vortex during winter. It is evident that a wind reversal is present in both cases, but differences in strength and timing are apparent.

In the lower mesosphere, both the noMEE and MEE run present a normal winter climatology until day  $-5$ . Below  $10^{-2}$  hPa, the zonal wind slows down from more than 40 m/s until it becomes westward from day 0. In the noMEE run the zonal wind stays westward until day 9, reaching a minimum of less than  $-40$  m/s. However, in the MEE case the westward wind is interrupted several times, first on day 3 as it turns eastward for two days, while it is still westward in the noMEE run. Finally, from day 5 until day 9, the winds reverse again, turning westward and reaching almost  $-40$  m/s between day 6 and day 8.

In the upper mesosphere, above  $10^{-2}$  hPa, the typical winter zonal wind is westward as shown for the first two weeks in Figure 2. The wind reversal associated with the SSW occurs already at day  $-5$  in the noMEE case, while it occurs later in the MEE case and with a weaker amplitude. Conversely, around the mesopause between  $10^{-4}$  and  $10^{-3}$  hPa, the eastward winds are stronger in the MEE case compared to the noMEE case. In particular, in the noMEE run the eastward reaches over 40 m/s from day 5 until day 8, a factor 2 larger compared to the MEE run. In summary, it is evident that the mesospheric zonal wind signatures during the SSW display different features in the MEE and noMEE case, indicating that MEE can somehow impact the dynamics of the mesosphere.

Figure 3 shows the zonal wind difference (upper left panel), the temperature difference (upper right panel), the NO relative difference (lower left panel), and the  $\text{O}_3$  difference (lower right panel) between the MEE and noMEE case. The zonal wind differences confirm that between day 3 and 9, the zonal wind discrepancies between both runs are larger than 20 m/s throughout the mesosphere and lower thermosphere region. Until day 13, zonal wind discrepancies larger than 20 m/s are still present between  $10^{-2}$  and  $10^{-4}$  hPa. Prior to the wind reversal, from day

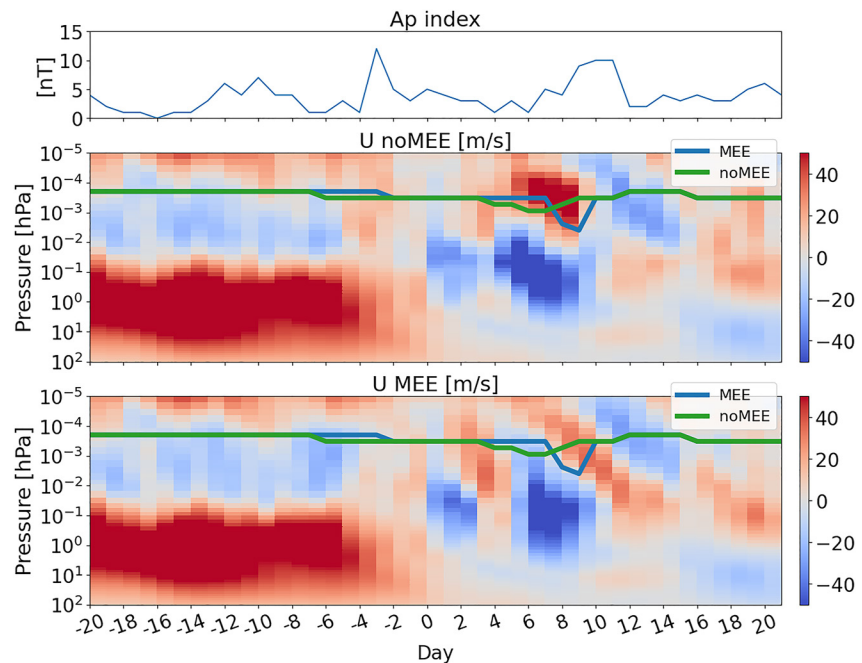


**Figure 2.** The upper plot corresponds to the zonal wind velocity for the noMEE run. The lower plot shows the zonal wind velocity for the Medium energy electrons (MEE) run. The red color represents positive velocities, associated with eastward winds, while blue represents negative velocities, associated with westward winds. The data is averaged over the latitude band 60–70°N with a daily resolution. The two colored lines represent the mesopause altitude (coldest altitude) for both runs, the blue line corresponds to the MEE run, and the green line to the noMEE run.

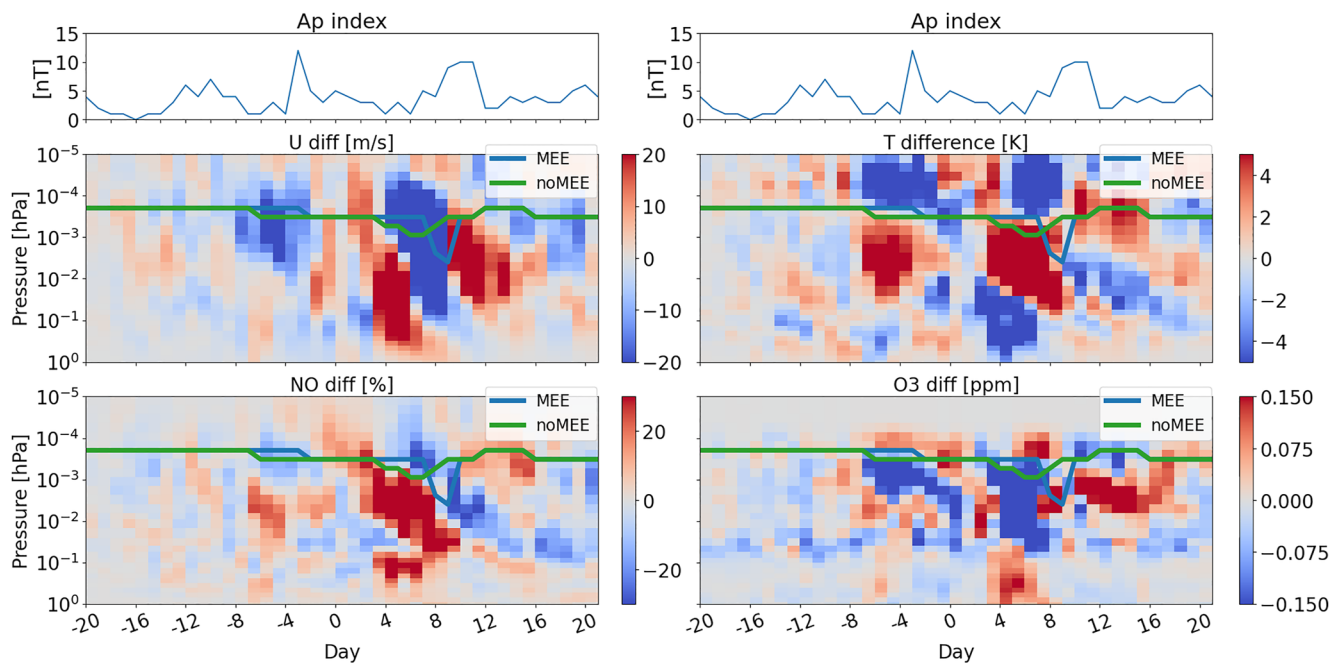


**Figure 3.** Upper plots (from left to right): Zonal wind velocity difference between the MEE and the noMEE run, and temperature difference between both runs. Bottom plots (from left to right): NO VMR relative difference, and  $O_3$  absolute difference. For all plots, the data is averaged over the latitude band 60–70°N with a daily resolution. The two colored lines represent the mesopause altitude (coldest altitude) for both runs, the blue line corresponds to the MEE run, and the green line to the noMEE run.

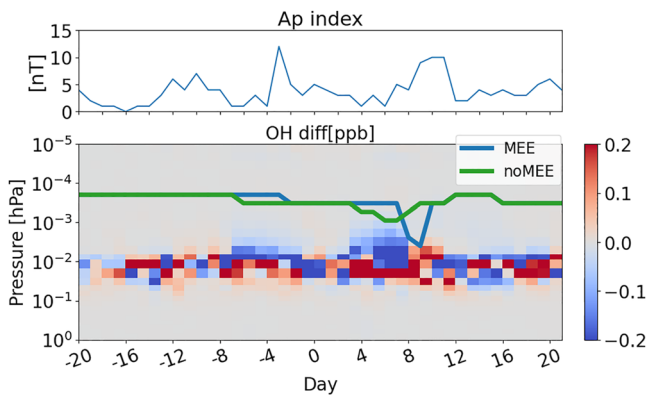


**Figure 4.** OH absolute difference, the data is averaged over the latitude band 60–70°N with a daily resolution. The two colored lines represent the mesopause altitude (coldest altitude) for both runs. The blue line corresponds to the Medium energy electrons (MEE) run, and the green line to the noMEE run.

–8 to day –3, negative zonal wind differences up to 20 m/s are persistently seen at altitudes around the mesopause, consistent with the late wind reversal found in the MEE run.

On day 3, there is a positive relative difference in the NO abundance around  $10^{-3}$  hPa between the MEE and noMEE case. The anomaly is transported downwards during the next few days. On day 9, there is, however, a relative NO decrease in the MEE run at around  $10^{-3}$  hPa, which is also transported downwards during the next few days. The noMEE run has less NO production throughout the mesosphere. The only process that can cause the noMEE to have more mesospheric NO is a change in the dynamics, either in the strength and/or timing of the residual transport. Specifically, the NO increase followed by a decrease seen in Figure 3 supports a time shift in the residual transport. Note, however, that the positive signal is stronger than the negative, which demonstrate overall contribution to the NO production by MEE.

During an SSW, NO typically decreases in the lower mesosphere, since the stratospheric wind reversal allow westerly gravity waves to break and deposit their momentum in the mesosphere and reduce the residual downward transport (Smith et al., 2011). After the SSW, when the zonal winds again turn eastward in the lower mesosphere/upper stratosphere, the downward transport is restored.

Based on Figure 2, this likely occurs for a short period of time already on day 3 for the MEE run, which coincides in time with the NO relative increase throughout the mesosphere seen in the MEE run in Figure 3. Furthermore, the NO relative increase in the noMEE run happens on day 9, which suggest a stronger downward transport in the noMEE run. The period coincides in time with an abrupt change in the mesospheric zonal wind in the MEE and noMEE model projections. The mesospheric zonal wind are less eastward in the MEE run compared to the noMEE run.

Temperature differences larger than 5K are evident from day 3 until day 9 in the upper mesosphere, consistent with adiabatic warming associated with the enhanced downward transport found for the NO VMR. The O<sub>3</sub> difference between the MEE and noMEE model projections might further contribute to warmer mesospheric temperature (less radiative cooling) in the MEE run. Before the SSW, temperature differences up to 5K are found from day –6 to day –3. This difference consists of warmer temperatures in the MEE run just below the mesopause, and colder temperatures above the mesopause. This dipole-like signal suggests that there might be a shift in the altitude where gravity waves deposit their energy. In fact, these temperature differences coincide in time with the negative zonal wind differences seen around the mesopause, suggesting greater westward gravity wave drag at this altitude in the MEE run. A confirmation of this hypothesis will require analysis of the gravity wave forcing, which is not currently available for the respective runs.

The overall picture of O<sub>3</sub> shows large changes occurring at the same time and location where dynamical changes take place. Furthermore, between  $10^{-1}$  and  $10^{-2}$  hPa, persistently less O<sub>3</sub> is obtained in the MEE run. Due to the absence of UV absorption during winter, O<sub>3</sub> works as a cooling agent (Brasseur & Solomon, 2005), meaning that a relative decrease in O<sub>3</sub> will lead to a relative increase in temperature. Persistently warmer temperatures around 2K are found in the MEE run between  $10^{-1}$  and  $10^{-2}$  hPa before day –8. These warmer temperatures translate into a less steep gradient in the lower mesosphere for the MEE run. A change in the temperature gradient will allow gravity waves to become convectively unstable and break at a different altitude compared to the noMEE case, which can potentially explain the following dynamical differences obtained between the noMEE and MEE runs.

The NO<sub>x</sub> catalytic cycle destroying O<sub>3</sub> is effective only below ~0.5 hPa, while the HO<sub>x</sub> catalytic cycle is effective already in the upper and middle mesosphere (Lary, 1997). Figure 4 shows the OH differences between the MEE and the noMEE case. It clearly displays a change confined roughly between  $10^{-1}$  and  $10^{-2}$  hPa, the same altitude where persistently less O<sub>3</sub> is found in the MEE run. It does, however, show no persistent increase throughout the mesosphere. There is, however, a tendency of a bipolar pattern with a positive response below the negative one. The negative change is consistent with increased downward transport of dry air, while the positive change is related to increased OH production. Considering that OH is given as VMR imply that the total amount of OH is increased in the MEE run compared to the noMEE run as expected. Moreover, the MEE produced OH will

be strongly affected by the respective change in transport in the two runs as previously discussed by Zawedde et al. (2016). Also, an unclear signal might be attributed to the time resolution as the lifetime of OH in the mesosphere is about hours (Brasseur & Solomon, 2005) while Figure 4 is based on a daily average.

#### 4. Summary

The existing theory on how EEP can change the atmospheric dynamics, assumes the indirect EEP impact on stratospheric  $O_3$  as the initial driver (Baumgaertner et al., 2011; Seppälä et al., 2013). The role of the direct MEE effect via mesospheric  $O_3$  depletion is, however, still unclear. This is partly due to model studies applied in free-running mode and/or analyzing the result on a monthly/seasonal time scale, which could cause the initial temperature response in the mesosphere to be concealed by the subsequent dynamical feedback.

This study applies the chemistry-climate model WACCM in SD-mode, nudging the atmospheric dynamics to the MERRA reanalysis. As such, it prevents realistic assessment of the feedback loops involving the stratosphere, but enables an isolated assessment of the mesospheric dynamical response to the MEE direct effect. This approach confirms notable changes in the mesospheric zonal wind and temperature due to MEE, which occur before and during an SSW in late January/early February. In line with the geomagnetic activity, the MEE case typically has more NO in the mesosphere than the noMEE case, as expected. There are, however, also periods in time when there is less NO throughout the mesosphere in the MEE case compared to the noMEE case. This NO deficit in the MEE case can only be explained by a reduction in the residual circulation transporting less NO from above.

Running the model in SD mode has the advantage of ensuring that both the MEE and noMEE case have the same stratospheric wave filtering, which implies that the same planetary and gravity waves are entering the lower mesosphere. Gravity waves are the main driver of the mesospheric dynamics and the upper branch of the Brewer-Dobson circulation. Hence, a dynamical change implies that the temperature gradient the propagating gravity waves encounter is different in the MEE and noMEE case. As such, the small initial change in the temperature gradient must be adequate to redistribute the gravity wave momentum deposition. The mesosphere lower thermosphere region is free-running, which ideally should be studied using multiple ensemble members. Hence, the absolute impact of the MEE direct effect on temperature and winds must be interpreted with some reservations. There is a risk that changes are an effect of non-linearity effects of the model and not solely related to the MEE forcing. Nevertheless, there are no other times or geographical regions displaying such differences in temperature or winds between the MEE and noMEE case. This strongly suggest that conditions shortly before and during an SSW provide a pivotal point in the model, where even a minor change in ozone and temperature, corresponding to a weak MEE forcing, can influence the mesospheric SSW signal.

Asikainen et al. (2020) demonstrated that EEP-related enhancement of the stratospheric polar vortex and other associated dynamical changes are seen only during winters when an SSW occurs and that the EEP-related changes are observed slightly before the SSW onset. This is consistent with the findings in this study. An initial weak temperature increase in the MEE case associated with the mesospheric  $O_3$  depletion is found 5–10 days before the SSW as shown in Figure 3. Furthermore, Asikainen et al. (2020) hypothesized that the increased planetary wave activity before the SSW favors enhanced wave-mean-flow interaction, which can dynamically amplify the initial polar vortex enhancement caused by the  $O_3$  loss. Our findings imply that this hypotheses may be expanded to also include gravity waves. In the MEE case, the zonal wind reversal is less pronounced, which demonstrates that the MEE direct effect can influence the Northern Hemisphere mesospheric dynamics during unstable atmospheric conditions. The SD run, cannot reveal if the imprint of the EEP direct effect extends to the stratosphere as the temperature and wind field are nudged by reanalysis data. However, the temperature and wind fields in Figure 3 are changed all the way to the nudged pressure level, including the transition layer, suggesting that the impact will not be limited to mesosphere in the case of a free running model projection.

The largest dynamical difference between the MEE and noMEE case coincides with a period with low geomagnetic activity, but also unstable atmospheric mean-flow conditions associated with an SSW. Other wintertime periods, characterized by significantly stronger MEE ionization, do not cause a similar temperature or dynamical signal in the mesosphere. It has been a common practice in the research field to group the polar winter response into a high and low geomagnetic activity and evaluate their difference as a potential EEP imprint (Seppälä et al., 2013). The implication of a necessary dynamical precondition for the EEP effect to take place overturns this methodology. This implies a non-linear dependence on the EEP ionization rates, where the threshold for

altering the dynamics varies concurrently with the dynamical preconditions. This is consistent with Salminen et al. (2019) which displays a non-linear tendency between the polar vortex zonal wind and the EPP flux levels.

Finally, these results imply that MEE and EEP in general are able to modulate the strength and timing of the SSW imprint in the mesosphere. As such, they support results by Salminen et al. (2020), who showed SSW occurrence rates being modulated by geomagnetic activity during the latter half of the 20th century. SSWs have a substantial impact on winter weather in the Northern Hemisphere by causing cold weather spells to North America and Europe (Baldwin et al., 2021). Including MEE, and EEP forcing in general, in Earth system models, can potentially improve seasonal and regional predictions of SSW impacts on populated regions and as such greatly benefit society. A final confirmation of this mechanism will require a more extensive model run including multiple ensemble members and/or scaled forcing to exclude potential non-linear artifacts of WACCM itself. Moreover, comparison with observations should be applied to validate which model projections best comply with for example, temperature observations by Microwave Limb Sounder on the AIM satellite on the Aura satellite.

### Data Availability Statement

The Whole Atmosphere Community Climate Model is freely available and can be used by the community (<https://escomp.github.io/CESM/versions/cesm2.2/html/introduction.html>). The specific model output can be found in the Norwegian data repository <https://dataverse.no/dataverse/uib> using the doi: <https://doi.org/10.18710/9KSAQR>.

### Acknowledgments

The research has been funded by the Norwegian Research Council (NRC) under contract 223252, 302040, and 300724. We would like to acknowledge high-performance computing support from Cheyenne provided by National Center for Atmospheric Research's Computational and Information Systems Laboratory.

### References

- Andersson, M. E., Verronen, P. T., Marsh, D. R., Päiväranta, S.-M., & Plane, J. M. C. (2016). Waccm-d—Improved modeling of nitric acid and active chlorine during energetic particle precipitation. *Journal of Geophysical Research: Atmospheres*, *121*(17), 10328–10341. <https://doi.org/10.1002/2015JD024173>
- Andersson, M. E., Verronen, P. T., Rodger, C. J., Clilverd, M. A., & Seppälä, A. (2014). Missing driver in the sun-Earth connection from energetic electron precipitation impacts mesospheric ozone. *Nature Communications*, *5*(1), 5197. <https://doi.org/10.1038/ncomms6197>
- Arsenovic, P., Rozanov, E., Stenke, A., Funke, B., Wissing, J., Mursula, K., et al. (2016). The influence of middle range energy electrons on atmospheric chemistry and regional climate. *Journal of Atmospheric and Solar-Terrestrial Physics*, *149*, 180–190. <https://doi.org/10.1016/j.jastp.2016.04.008>
- Asikainen, T., Salminen, A., Maliniemi, V., & Mursula, K. (2020). Influence of enhanced planetary wave activity on the polar vortex enhancement related to energetic electron precipitation. *Journal of Geophysical Research: Atmospheres*, *125*(9), e2019JD032137. <https://doi.org/10.1029/2019JD032137>
- Baldwin, M. P., Ayarzagüena, B., Birner, T., Butchart, N., Butler, A. H., Charlton-Perez, A. J., et al. (2021). Sudden stratospheric warmings. *Reviews of Geophysics*, *59*(1), e2020RG000708. <https://doi.org/10.1029/2020RG000708>
- Baumgaertner, A. J. G., Seppälä, A., Jöckel, P., & Clilverd, M. A. (2011). Geomagnetic activity related NO<sub>x</sub> enhancements and polar surface air temperature variability in a chemistry climate model: Modulation of the NAM index. *Atmospheric Chemistry and Physics*, *11*(9), 4521–4531. <https://doi.org/10.5194/acp-11-4521-2011>
- Brasseur, G., & Solomon, S. (2005). *Aeronomy of the middle atmosphere: Chemistry and physics of the stratosphere and mesosphere*. <https://doi.org/10.1007/1-4020-3824-0>
- Codrescu, M. V., Fuller-Rowell, T. J., Roble, R. G., & Evans, D. S. (1997). Medium energy particle precipitation influences on the mesosphere and lower thermosphere. *Journal of Geophysical Research*, *102*(A9), 19977–19987. <https://doi.org/10.1029/97JA01728>
- Gottelman, A., Mills, M. J., Kinnison, D. E., Garcia, R. R., Smith, A. K., Marsh, D. R., et al. (2019). The whole atmosphere community climate model version 6 (WACCM6). *Journal of Geophysical Research: Atmospheres*, *124*(23), 12380–12403. <https://doi.org/10.1029/2019JD030943>
- Guttu, S., Orsolini, Y., Stordal, F., Limpasuvan, V., & Marsh, D. R. (2020). Waccm simulations: Decadal winter-to-spring climate impact on middle atmosphere and troposphere from medium energy electron precipitation. *Journal of Atmospheric and Solar-Terrestrial Physics*, *209*, 105382. <https://doi.org/10.1016/j.jastp.2020.105382>
- Hurrell, J. W., Holland, M. M., Gent, P. R., Ghan, S., Kay, J. E., Kushner, P. J., et al. (2013). The community Earth system model: A framework for collaborative research. *Bulletin of the American Meteorological Society*, *94*(9), 1339–1360. <https://doi.org/10.1175/BAMS-D-12-00121.1>
- Jia, Y., Zhang, S., Yi, F., Huang, C. M., Huang, K. M., Gong, Y., & Gan, Q. (2016). Variations of kelvin waves around the t1 region during the stratospheric sudden warming events in the northern hemisphere winter. *Annales Geophysicae*, *34*(3), 331–345. <https://doi.org/10.5194/angeo-34-331-2016>
- Kunz, A., Pan, L. L., Konopka, P., Kinnison, D. E., & Tilmes, S. (2011). Chemical and dynamical discontinuity at the extratropical tropopause based on start08 and waccm analyses. *Journal of Geophysical Research*, *116*(D24). <https://doi.org/10.1029/2011JD016686>
- Lary, D. J. (1997). Catalytic destruction of stratospheric ozone. *Journal of Geophysical Research*, *102*(D17), 21515–21526. <https://doi.org/10.1029/97JD00912>
- Maliniemi, V., Asikainen, T., Salminen, A., & Mursula, K. (2019). Assessing north atlantic winter climate response to geomagnetic activity and solar irradiance variability. *The Quarterly Journal of the Royal Meteorological Society*, *145*(725), 3780–3789. <https://doi.org/10.1002/qj.3657>
- Maliniemi, V., Marsh, D. R., Nesse Tyssøy, H., & Smith-Johnsen, C. (2020). Will climate change impact polar nox produced by energetic particle precipitation? *Geophysical Research Letters*, *47*(9), e2020GL087041. <https://doi.org/10.1029/2020GL087041>
- Marsh, D. R., Mills, M. J., Kinnison, D. E., Lamarque, J.-F., Calvo, N., & Polvani, L. M. (2013). Climate change from 1850 to 2005 simulated in cesm1(waccm). *Journal of Climate*, *26*(19), 7372–7391. <https://doi.org/10.1175/JCLI-D-12-00558.1>
- Marsh, D. R., Solomon, S. C., & Reynolds, A. E. (2004). Empirical model of nitric oxide in the lower thermosphere. *Journal of Geophysical Research*, *109*(A7), A07301. <https://doi.org/10.1029/2003JA010199>



- Meraner, K., & Schmidt, H. (2018). Climate impact of idealized winter polar mesospheric and stratospheric ozone losses as caused by energetic particle precipitation. *Atmospheric Chemistry and Physics*, 18(2), 1079–1089. <https://doi.org/10.5194/acp-18-1079-2018>
- Mironova, I. A., Aplin, K. L., Arnold, F., Bazilevskaia, G. A., Harrison, R. G., Krivolutsky, A. A., et al. (2015). Energetic particle influence on the Earth's atmosphere. *Space Science Reviews*, 194(1–4), 1–96. <https://doi.org/10.1007/s11214-015-0185-4>
- Randall, C. E., Harvey, V. L., Singleton, C. S., Bailey, S. M., Bernath, P. F., Codrescu, M., et al. (2007). Energetic particle precipitation effects on the southern hemisphere stratosphere in 1992–2005. *Journal of Geophysical Research*, 112(D8), D08308. <https://doi.org/10.1029/2006JD007696>
- Rienecker, M. M., Suarez, M. J., Gelaro, R., Todling, R., Bacmeister, J., Liu, E., et al. (2011). Merra: Nasa's modern-era retrospective analysis for research and applications. *Journal of Climate*, 24(14), 3624–3648. <https://doi.org/10.1175/JCLI-D-11-00015.1>
- Roble, R. G., Ridley, E. C., & Dickinson, R. E. (1987). On the global mean structure of the thermosphere. *Journal of Geophysical Research*, 92(A8), 8745–8758. <https://doi.org/10.1029/JA092iA08p08745>
- Salminen, A., Asikainen, T., Maliniemi, V., & Mursula, K. (2019). Effect of energetic electron precipitation on the northern polar vortex: Explaining the qbo modulation via control of meridional circulation. *Journal of Geophysical Research: Atmospheres*, 124(11), 5807–5821. <https://doi.org/10.1029/2018JD029296>
- Salminen, A., Asikainen, T., Maliniemi, V., & Mursula, K. (2020). Dependence of sudden stratospheric warmings on internal and external drivers. *Geophysical Research Letters*, 47(5), e2019GL086444. <https://doi.org/10.1029/2019GL086444>
- Semeniuk, K., Fomichev, V. I., McConnell, J. C., Fu, C., Melo, S. M. L., & Usoskin, I. G. (2011). Middle atmosphere response to the solar cycle in irradiance and ionizing particle precipitation. *Atmospheric Chemistry and Physics*, 11(10), 5045–5077. <https://doi.org/10.5194/acp-11-5045-2011>
- Seppälä, A., Lu, H., Clilverd, M. A., & Rodger, C. J. (2013). Geomagnetic activity signatures in wintertime stratosphere wind, temperature, and wave response. *Journal of Geophysical Research: Atmospheres*, 118(5), 2169–2183. <https://doi.org/10.1002/jgrd.50236>
- Sinnhuber, M., Nieder, H., & Wieters, N. (2012). Energetic particle precipitation and the chemistry of the mesosphere/lower thermosphere. *Surveys in Geophysics*, 33(6), 1281–1334. <https://doi.org/10.1007/s10712-012-9201-3>
- Smith, A. K., Garcia, R. R., Marsh, D. R., & Richter, J. H. (2011). Waccm simulations of the mean circulation and trace species transport in the winter mesosphere. *Journal of Geophysical Research*, 116(D20), D20115. <https://doi.org/10.1029/2011JD016083>
- Solomon, S., Crutzen, P. J., & Roble, R. G. (1982). Photochemical coupling between the thermosphere and the lower atmosphere: 1. Odd nitrogen from 50 to 120 km. *Journal of Geophysical Research*, 87(C9), 7206. <https://doi.org/10.1029/JC087iC09p07206>
- van de Kamp, M., Seppälä, A., Clilverd, M. A., Rodger, C. J., Verronen, P. T., & Whittaker, I. C. (2016). A model providing long-term data sets of energetic electron precipitation during geomagnetic storms. *Journal of Geophysical Research: Atmospheres*, 121(20), 12520–12540. <https://doi.org/10.1002/2015JD024212>
- Verronen, P. T., Andersson, M. E., Marsh, D. R., Kovács, T., & Plane, J. M. C. (2016). Waccm-d—Whole atmosphere community climate model with d-region ion chemistry. *Journal of Advances in Modeling Earth Systems*, 8(2), 954–975. <https://doi.org/10.1002/2015MS000592>
- Zawedde, A. E., Nesse Tyssøy, H., Hibbins, R., Espy, P. J., Ødegaard, L.-K. G., Sandanger, M. I., & Stadsnes, J. (2016). The impact of energetic electron precipitation on mesospheric hydroxyl during a year of solar minimum. *Journal of Geophysical Research: Space*, 121(6), 5914–5929. <https://doi.org/10.1002/2016JA022371>
- Zawedde, A. E., Nesse Tyssøy, H., Stadsnes, J., & Sandanger, M. I. (2018). The impact of energetic particle precipitation on mesospheric oh – Variability of the sources and the background atmosphere. *Journal of Geophysical Research: Space*, 123(7), 5764–5789. <https://doi.org/10.1029/2017JA025038>
- Zawedde, A. E., Nesse Tyssøy, H., Stadsnes, J., & Sandanger, M. I. (2019). Are eep events important for the tertiary ozone maximum? *Journal of Geophysical Research: Space*, 124(7), 5976–5994. <https://doi.org/10.1029/2018JA026201>